Thermo-viscoelastic homogenization of 3D woven composites with time-dependent expansion coefficients

Martin Hirsekorn, Lionel Marcin, Thierry Godon

Highlights

Thermo-viscoelastic homogenization of 3D woven composites with time-dependent expansion coefficients

Martin Hirsekorn, Lionel Marcin, Thierry Godon

- Viscoelastic constitutive behavior with time-dependent thermal expansion coefficients
- Effect of stress relaxation on the average thermal expansion of a 3D woven composite
- Viscoelastic homogenization of thermal expansion and chemical shrinkage coefficients
- Validation of the homogenization method by full-scale Finite Element simulations

Thermo-viscoelastic homogenization of 3D woven composites with time-dependent expansion coefficients

Martin Hirsekorn[a,*], Lionel Marcin[b], Thierry Godon[b]

[a] *DMAS, ONERA, Université Paris Saclay, 92322 Châtillon, France*
[b] *Safran Aircraft Engines, Rond point René Ravaud, 77550 Moissy Cramayel, France*

Abstract

Stress relaxation in the viscoelastic matrix influences the evolution of thermal expansion and chemical shrinkage of polymer composites. Its effects are included into a viscoelastic model of the generalized Maxwell type by means of time-dependent thermal expansion and chemical shrinkage coefficients. A homogenization strategy is proposed to obtain these coefficients of the composite from the constituent behaviors, taking into account the viscoelastic effects. The homogenized behavior is validated by full-scale finite element simulations. It reproduces features such as sign changes of the thermal strain rate close to the glass transition temperature and thermal creep effects, which can have an important impact on the residual stress formation in composites, but are not taken into account by classical thermo-elastic homogenization methods.

Keywords: Homogenization, Time-dependent, Thermoelastic, Viscoelastic, Composite materials, Relaxation, Thermal expansion, Chemical shrinkage

1. Introduction

The distinguishing advantage of composites of combining dissimilar constituents to form a material with superior characteristics inevitably comes along with the issue of residual stresses, which may affect shape and integrity of the composite part, but in some cases may also be beneficial to its performance. In composites made of a reinforcement of strong and

*Corresponding Author
Email address: martin.hirsekorn@onera.fr (Martin Hirsekorn)

stiff fibers (*e.g.,* glass or carbon) held together by a thermosetting polymer matrix, the main factor is the mismatch in the coefficient of thermal expansion (CTE) between the fibers and the matrix, causing residual stresses mainly during the cooling phase at the end of the cure cycle [White and Kim, 1998; Wisnom et al., 2006; Zobeiry et al., 2016]. Another important contribution comes from the volume loss of the thermosetting resin with increasing degree of cure (called *chemical* or *cure shrinkage* [Wisnom et al., 2006; Russell et al., 2000; Billotte et al., 2013]), while the fibers are not influenced by the polymerization of the matrix. The generated stresses depend on the mechanical behavior of the constituents. While glass or carbon fibers can be considered in a good approximation as linear elastic and independent of temperature over the range of the cure cycle, the behavior of the matrix strongly depends on both temperature and degree of cure [O'Brien et al., 2001; Zarrelli et al., 2010; Courtois et al., 2018], with transitions between the glassy and the rubbery state. Furthermore, the behavior of the matrix is viscoelastic [O'Brien et al., 2001; Courtois et al., 2018; Kim and White, 1996], which makes strain and stress evolve in time even when temperature and cure are constant.

A large number of modeling strategies were published for the prediction of residual stresses in thermoset composites. Some works focus on computationally efficient simplified constitutive behaviors, like Cure Hardening Instantaneously Linear Elastic (CHILE) [Johnston et al., 2001], path-dependent [Svanberg and Holmberg, 2004], or pseudo-viscoelastic (PVE) [Zobeiry et al., 2010] models. These methods approximate the final stress and strain state, but neglect the continuous evolution in time due to creep and relaxation effects within the composite. They can give accurate predictions of residual stresses and the post-cure shape of composite parts, but only for materials and cure cycles during which the modulus increases all the time [Zobeiry et al., 2016]. Viscoelastic models are computationally more expensive due to the more complex formulation and the large number of internal variables that have to be stored, but since they take into account creep and relaxation effects, they are more appropriate to give accurate predictions of residual stresses for arbitrary cure cycles. For example, Benavente et al. [2017] showed that the distortion of asymmetric 3D woven interlock composites evolves in time during post-curing, and that this effect is caused by

creep strains, which have an important impact even below the glass transition temperature T_g of the resin.

In most studies that use viscoelastic approaches to predict residual stresses, the viscoelastic behavior of the composite is modeled [*e.g.,* White and Kim, 1998; Zhang et al., 2016; Ding et al., 2016] without looking at the lower scales. In some recent works, the composite behavior is derived from the behavior of the constituents by homogenization [Benavente et al., 2018; Hirsekorn et al., 2018; Courtois et al., 2019; Trofimov et al., 2021]. In the case of textile composites, two scale changes are needed to obtain the homogenized behavior of the composite [Hirsekorn et al., 2018]. The first homogenization step determines the behavior of the consolidated tows from the elastic behavior of the fiber and the viscoelastic behavior of the matrix, using a Representative Volume Element (RVE) at the microscopic scale (parallel fibers embedded in a matrix, in most cases either in a periodic hexagonal array or random distribution, with periodic boundary conditions (PBC)). In the second step, the behavior of the composite is determined from the viscoelastic behaviors of the matrix and the tows (with potentially different fiber volume fractions in different tows), using a RVE at the mesoscopic scale, which takes into account the weaving architecture of the composite.

In the cited works, a time-dependent viscoelastic behavior is used for the average mechanical behavior of the composite, but time-independent average CTE and coefficients of chemical shrinkage (CCS). However, it is easy to imagine that if residual stresses arise in the matrix due to a temperature change or due to chemical shrinkage, these stresses cause a gradual evolution of the matrix strain in time, due to its viscoelastic behavior. In interaction with the fibers, the residual stresses and also the average strain of the composite evolve in time. In a viscoelastic model of the composite with time-independent CTE and CCS, these effects are not taken into account, as creep and relaxation are only caused by mechanical loads applied to the composite. Temperature changes, however, only cause an immediate thermal expansion, which does not further evolve when the temperature is kept constant. While this consideration shows that there must be time-dependent thermal expansion effects in composite materials with time-dependent constituent behaviors, only few studies actually proposed time-dependent CTE [*e.g.,* Zocher et al., 1997; Sawant and Muliana, 2008; Pet-

termann and DeSimone, 2018]. Experimental evidence of the mentioned effects was found in composites [Benavente et al., 2017] and also in other materials, such as concrete [BaÅ$\frac{3}{4}$ant, 1970]. Logically, chemical shrinkage in composites with viscoelastic constituents should also cause a time-dependent reaction.

In this paper, we use a viscoelastic model with time-dependent CTE and CCS, based on the work of Sawant and Muliana [2008] and Pettermann and DeSimone [2018]. We show how the parameters of such a model can be obtained by homogenization from the mechanical behavior of the constituents (elastic for the fiber and temperature and cure-dependent viscoelastic for the matrix [Courtois et al., 2018]) with time-independent expansion coefficients for the fibers and the matrix. The constitutive models and a numerical integration method for the viscoelastic behavior and the time-dependent expansion coefficients are presented in section 2. The homogenization technique based on the Laplace-Carson (LC) transform is described in section 3. In section 4, it is shown how to apply the proposed method to the case of a thermosetting matrix composite with a 3D woven reinforcement made of carbon fibers. The results presented in section 5 show that there is indeed significant time-dependence of the homogenized thermal expansion and chemical shrinkage of the composite. Taking into account the influence of temperature on the viscoelastic behavior of the matrix, the strain evolution of the composite when heated up to its T_g is simulated by full-scale Finite Element (FE) simulations and the homogenized behavior. The results are in excellent agreement, showing that the homogenized behavior of the composite takes into account the stress relaxation and temperature effects at the lower scales.

2. Viscoelastic constitutive behavior with time-dependent expansion coefficients

Zocher et al. [1997] included time-dependent effects of thermal expansion into the classical integral form of viscoelasticity, which expresses stress as the Stieltjes convolution of a fourth-order tensor of anisotropic relaxation moduli $\underline{\underline{E}}$ with the strain tensor $\underline{\varepsilon}$ over a reduced time ξ (first integral in Eq. 1). The influence of time-dependent thermal expansion on stress is expressed as a Stieltjes convolution of a second-order tensor $\underline{\beta}^{th}$ with temperature, which is

subtracted from the mechanical stress:

$$\underline{\sigma}(\xi) = \int_{-\infty}^{\xi} \underline{\underline{E}}(\xi - \xi') : \frac{\partial \underline{\varepsilon}(\xi')}{\partial \xi'} d\xi' - \int_{-\infty}^{t} \underline{\beta}^{th}(\xi - \xi') \frac{\partial T(\xi')}{\partial \xi'} d\xi' \tag{1}$$

The reduced time is defined as

$$\xi(t) = \int_{-\infty}^{t} \frac{1}{a_T(t')} dt', \quad \xi' = \xi(t') \tag{2}$$

where a_T is the shift factor of the time-temperature superposition principle.

Sawant and Muliana [2008] employed an additive decomposition of strain into a mechanical (viscoelastic) part $\underline{\varepsilon}^{ve}$ and a thermal part $\underline{\varepsilon}^{th}$ as in the classical formulation of thermo-viscoelasticity with time-independent CTE. The viscoelastic strain is given by the Stieltjes convolution of a fourth-order tensor of anisotropic creep compliances with the stress tensor. The thermal strain is the Stieltjes convolution of the second-order tensor $\underline{\alpha}^{th}$ of time-dependent CTE with temperature. Pettermann and DeSimone [2018] used a combination of both formulations to write stress as

$$\underline{\sigma}(\xi) = \int_{-\infty}^{\xi} \underline{\underline{E}}(\xi - \xi') : \frac{\partial \underline{\varepsilon}^{ve}(\xi')}{\partial \xi'} d\xi' \tag{3}$$

with

$$\underline{\varepsilon}^{th}(\xi) = \int_{-\infty}^{\xi} \underline{\alpha}^{th}(\xi - \xi') \frac{\partial T(\xi')}{\partial \xi'} d\xi' \tag{4}$$

Since relaxation and creep based integral forms are interconvertible [Park and Schapery, 1999; Schapery and Park, 1999], all three formulations can be converted into each other, if the tensor $\underline{\beta}^{th}$ of Zocher et al. [1997] is given by the Stieltjes convolution of the relaxation tensor $\underline{\underline{E}}$ with the time-dependent CTE $\underline{\alpha}^{th}$

Note that for time-independent $\underline{\alpha}^{th}$, the integral form of Eq. (4) resolves to the differential form of the CTE

$$d\underline{\varepsilon}^{th} = \underline{\alpha}^{th} dT \tag{5}$$

The numerical implementation of the integral form of viscoelasticity is largely simplified if the relaxation modulus can be written in terms of a Prony series [Zocher et al., 1997; Sawant and Muliana, 2008; Hirsekorn et al., 2010, 2011], *i.e.,*

$$\underline{\underline{E}}(\xi - \xi') = \underline{\underline{E}}_{\infty} + \sum_{k=1}^{N} \underline{\underline{E}}_k \mathrm{e}^{-\frac{\xi - \xi'}{\tau_k}} \tag{6}$$

where τ_k is called the relaxation time of the k^{th} relaxation mechanism. In the case of thermo-rheologically simple materials, in which the coefficients $\underline{\underline{E}}_k$ are constants, Eq. (3) resolves to

$$\underline{\sigma}(\xi) = \left(\underline{\underline{E}}_\infty + \sum_{k=1}^{N} \underline{\underline{E}}_k \right) : \underline{\varepsilon}^{ve}(\xi) - \sum_{k=1}^{N} \underline{\underline{E}}_k : \varepsilon_k^{ve}(\xi) \tag{7}$$

with the tensorial internal variables ε_k^{ve} accounting for the strain history [Sawant and Muliana, 2008]. Their evolution with the reduced time follows differential equations of the form

$$\frac{d\underline{\varepsilon}_k^{ve}(\xi)}{d\xi} = \frac{1}{\tau_k} \left(\underline{\varepsilon}^{ve}(\xi) - \underline{\varepsilon}_k^{ve}(\xi) \right) \tag{8}$$

These equations correspond to a 3D formulation of a generalized Maxwell model. Note that if the principle of time-temperature-cure superposition [Zarrelli et al., 2010; Courtois et al., 2018; Kim and White, 1996; Ding et al., 2016] can be used, *i.e.,* if the viscoelastic behavior depends on temperature and degree of cure only through the shift factor a_T defined in Eq. (2), the derivative with the reduced time in these differential equations can be replaced by a derivative with the real time if the relaxation times τ_k are multiplied by the shift factor. Eq. (8) then refers to the evolution of the internal variables in time, and the arguments with the reduced time are replaced by the respective time argument in the equations above.

The same procedure can be applied to the time-dependent $\underline{\alpha}^{th}$ [Pettermann and DeSimone, 2018] (for convenience we use a different sign convention):

$$\underline{\alpha}^{th}(\xi - \xi', T(\xi'), c(\xi')) = \underline{\alpha}_\infty^{th}(T(\xi'), c(\xi')) - \sum_{k=1}^{N} \underline{\alpha}_k^{th}(T(\xi'), c(\xi')) \mathrm{e}^{-\frac{\xi - \xi'}{\tau_k}} \tag{9}$$

Here, we allow for temperature and cure depending tensors $\underline{\alpha}_\infty^{th}$ and $\underline{\alpha}_k^{th}$. Note that this dependence refers to the moment of the change of temperature (ξ'). The effect in time of this temperature change is described by the Prony series.

We use the differential form of the CTE (5) and obtain the thermal strain by integration over the reduced time ξ'

$$\underline{\varepsilon}^{th}(\xi) = \int_{-\infty}^{\xi} \underline{\alpha}^{th}(\xi - \xi', T(\xi'), c(\xi')) \frac{\partial T(\xi')}{\partial \xi'} d\xi' + \lim_{\xi' \to -\infty} \underline{\varepsilon}^{th}(\xi') \tag{10}$$

If we express the thermal strain with respect to the state of the material at the beginning of history ($\xi' \to -\infty$), we can set the last term of the equation to zero. If we define

$$\underline{\varepsilon}_k^{th}(\xi) = \int_{-\infty}^{\xi} \underline{\alpha}_k^{th}(T(\xi'), c(\xi'))\mathrm{e}^{-\frac{\xi-\xi'}{\tau_k}} \frac{\partial T(\xi')}{\partial \xi'} d\xi' \tag{11}$$

and hence

$$\frac{d\underline{\varepsilon}_k^{th}(\xi)}{d\xi} = \underline{\alpha}_k^{th}(T(\xi), c(\xi))\frac{\partial T(\xi)}{\partial \xi} - \frac{1}{\tau_k}\underline{\varepsilon}_k^{th}(\xi) \tag{12}$$

inserting Eq. (9) into Eq. (10) and then differentiating yields

$$\frac{d\underline{\varepsilon}^{th}(\xi)}{d\xi} = \left(\underline{\alpha}_\infty^{th}(T(\xi), c(\xi)) - \sum_{k=1}^{N} \underline{\alpha}_k^{th}(T(\xi), c(\xi))\right) \frac{dT(\xi)}{d\xi} - \sum_{k=1}^{N} \frac{1}{\tau_k}\varepsilon_k^{th}(\xi) \tag{13}$$

The tensorial internal variables ε_k^{th} account for the history of temperature and the CTE. Their evolution follows the differential equations (12), which are similar to the evolution equations of the strain history variables. Like for the strain history variables, these equations can also be converted into differential equations in time by multiplication of the relaxation times with the shift factor.

Exactly the same formalism can be used to take into account the time-dependent effects of a change in degree of cure on the evolution of the strain $\underline{\varepsilon}^{ch}$ attributed to chemical shrinkage. The effect of chemical shrinkage enters the viscoelastic behavior by means of a decomposition of the total strain into a viscoelastic part $\underline{\varepsilon}^{ve}$, a thermal part $\underline{\varepsilon}^{th}$, and a chemical part $\underline{\varepsilon}^{ch}$:

$$\underline{\varepsilon} = \underline{\varepsilon}^{ve} + \underline{\varepsilon}^{th} + \underline{\varepsilon}^{ch} \tag{14}$$

For numerical integration of the constitutive equations in a FE code, we assume that the evolution of strain, CTE, and CCS over a given time step is linear. With this approximation, the evolution equations of the internal variables can be solved analytically to obtain their increments over the time step [Zocher et al., 1997; Hirsekorn et al., 2011]. More details on the incremental procedure are given in Appendix A.

3. Thermo-viscoelastic homogenization using the Laplace-Carson transform

3.1. Material behavior in the Laplace-Carson space

The LC-transform of a function f of the reduced time ξ is defined as

$$\hat{f}(p) = p \int_0^\infty f(\xi) \mathrm{e}^{-p\xi} d\xi \tag{15}$$

As described in Hirsekorn et al. [2018], the LC-transform of the integral form of the viscoelastic behavior given in Eq. (3) is given by

$$\hat{\underline{\sigma}}(p) = \hat{\underline{\underline{E}}}(p) : \hat{\underline{\varepsilon}}^{ve}(p) \tag{16}$$

Likewise, the LC-transform of Eq. (4) is

$$\hat{\underline{\varepsilon}}^{th}(p) = \hat{\underline{\alpha}}^{th}(p)\hat{T}(p) \tag{17}$$

In the LC-transform space, the constitutive behavior presented in section 2 takes the form of a thermo-elastic behavior that depends on the transform parameter p. The proposed homogenization strategy thus consists of the following steps:

- Calculate the LC-transform of the relaxation moduli, CTE, and CCS of each constituent
- Determine the LC-transform of the homogenized relaxation moduli, CTE, and CCS by thermo-elastic homogenization
- Apply the inversion of the LC-transform to obtain the coefficients of the time-dependent relaxation moduli, CTE, and CCS of the homogenized behavior in time space

We assume in the following that the relaxation moduli of the constituent materials as well as of the homogenized behavior can well be fitted by a Prony series of the form of Eq. 6 with *a priori* fixed relaxation times of one per decade on the logarithmic time scale. If the coefficients of the Prony series plotted against the relaxation times lie on a smooth curve without significant oscillations between adjacent relaxation times, the relaxation times can

be freely chosen, as long as there is at least one relaxation time per decade. It is then still possible to well fit the relaxation moduli by a Prony series with these freely chosen relaxation times. Under these assumptions, we take the same relaxation times for all constituents and for the homogenized behavior [Hirsekorn et al., 2018].

Of course, this is only an approximation to the exact homogenized behavior. Once the relaxation times of the constituents are fixed, the relaxation times of the analytically determined homogenized behavior are, in general, different from those of the constituents, as shown by Beurthey and Zaoui [2000]. However, the results obtained in Hirsekorn et al. [2018] show that for the material treated in this article, the relaxation spectra are sufficiently continuous such that this procedure yields an accurate approximation of the homogenized behavior obtained with full-scale FE simulations.

The LC-transform of the Prony-decomposition of the relaxation moduli (Eq. 6) at a given transform parameter p_i can be written as

$$\hat{\underline{\underline{E}}}(p_i) = \underline{\underline{E}}_{\infty} + \sum_{k=1}^{N} \mathcal{L}_{ik} \underline{\underline{E}}_k \tag{18}$$

where N is the number of relaxation times used to reproduce the viscoelastic spectrum. The LC-transform matrix is given by

$$\mathcal{L}_{ik} = \frac{p_i}{p_i + \frac{1}{\tau_k}} \tag{19}$$

Likewise, the LC-transform of the time-dependent CTE is

$$\hat{\underline{\alpha}}^{th}(p_i, T, c) = \underline{\alpha}^{th}_{\infty}(T, c) + \sum_{k=1}^{N} \mathcal{L}_{ik} \left(-\underline{\alpha}^{th}_{k}(T, c) \right) \tag{20}$$

The LC-transform of the CTE (and in the same way of the CCS) is calculated for a given temperature and degree of cure. The homogenization procedure thus yields the coefficients of the homogenized time-dependent CTE and CCS at that temperature and degree of cure. By homogenization of the CTE and CCS at various temperatures and degrees of cure covering the ranges of interest and interpolating the homogenized coefficients, the temperature and cure dependence of the homogenized material can be obtained (see section 3.2).

Eqs. (18) and (20) take the form of equation systems with the coefficients of the LC-transform matrix given by Eq. (19). The inversion of the LC-transform thus corresponds to

the solution of these equation systems for the unknowns $\underline{\underline{E}}_k$ and $\underline{\alpha}_k^{th}(T,c)$, respectively. The tensors $\underline{\underline{E}}_\infty$ and $\underline{\alpha}_\infty^{th}(T,c)$ can be obtained directly from thermo-elastic homogenization of the LC-transforms for $p=0$. In addition, the thermo-elastic homogenization is carried out for M different p_i, such that the LC-transform matrix becomes a $M \times N$-matrix. From this we can see that we need $M \geq N$ different p_i, one of which is usually $p=\infty$ (corresponding to the instantaneous behavior). If $M > N$, the optimum solution of the associated least-squares problem is calculated (see section 3.3). This problem corresponds to a least-squares fit of Eq. (18) to the LC-transform of the homogenized behavior, of which we calculate M points at the chosen p_i by thermo-elastic homogenization. The more points p_i, the better we describe the LC-transform of the homogenized behavior. However, this does not necessarily mean that we add more information. In fact, the condition of the least-squares problem and thus the accuracy of the solution is influenced by the choice of the p_i. The solution is thus not unique but depends on the choice of the p_i. The optimum choice for inversion algorithms of the LC-transform that are based on approximations of the solution in time space by Prony series was analyzed by Lévesque et al. [2007]. Some indications for the present method can be found in [Hirsekorn et al., 2018].

3.2. Thermo-elastic homogenization

The concept of thermo-elastic homogenization is well known, but the equations are briefly recalled here in order to explain the proposed methodology. In the following, an upper bar will identify an average property, and properties without upper bar are local properties. Angle brackets $\langle \cdots \rangle$ denote volume averaging.

The strain localization tensor $\underline{\underline{\hat{A}}}$ is defined as the tensor relating the local strain change $\hat{\underline{\varepsilon}}'$ due to an applied mechanical load to the global average mechanical strain $\hat{\bar{\underline{\varepsilon}}}^{ve}$ caused by this load:

$$\hat{\underline{\varepsilon}}'(\vec{x},p) = \underline{\underline{\hat{A}}}(\vec{x},p) : \hat{\bar{\underline{\varepsilon}}}^{ve} \tag{21}$$

Here, the hat indicates that the homogenization acts on LC-transforms.

Likewise, the stress concentration tensor $\underline{\underline{\hat{B}}}$ is defined as

$$\hat{\underline{\sigma}}'(\vec{x},p) = \underline{\underline{\hat{B}}}(\vec{x},p) : \hat{\underline{\sigma}} \tag{22}$$

where $\hat{\underline{\sigma}}$ is the global average stress and $\hat{\underline{\sigma}}'$ the local stress caused by $\hat{\underline{\sigma}}$. Note that while the global stress $\hat{\underline{\sigma}}$ is only caused by the mechanical load, the global strain $\hat{\underline{\varepsilon}}$ is composed of a part due to the mechanical load $\hat{\underline{\varepsilon}}^{ve}$ and a part due to thermal expansion (and possibly a part due to chemical shrinkage).

In a linear elastic material, these tensors can be determined by FE analysis, if 6 linear independent global strains (or stresses) are consecutively applied to the RVE. If we write these 6 linear independent global strain states in Kelvin notation as columns next to each other, we obtain a full-rank 6×6 matrix that we will denote by $\hat{\underline{\underline{\varepsilon}}}^{ve}$. The local strains obtained from the FE analyses are likewise arranged in Kelvin notation in 6×6 matrices $\hat{\underline{\underline{\varepsilon}}}'$. The same is done for the local stresses $\hat{\underline{\underline{\sigma}}}'$ and the average stress $\hat{\underline{\underline{\sigma}}}$. In a linear elastic material with a strictly positive definite stiffness tensor, the matrix $\hat{\underline{\underline{\sigma}}}$ also has full rank and can thus be inverted.

We therefore can obtain the strain localization tensor at each integration point from the solution of the 6 FE problems from

$$\hat{\underline{\underline{A}}}(\vec{x}, p) = \hat{\underline{\underline{\varepsilon}}}'(\vec{x}, p) : \left(\hat{\underline{\underline{\varepsilon}}}^{ve}\right)^{-1} \tag{23}$$

and the stress concentration tensor from

$$\hat{\underline{\underline{B}}}(\vec{x}, p) = \hat{\underline{\underline{\sigma}}}'(\vec{x}, p) : \left(\hat{\underline{\underline{\sigma}}}\right)^{-1} \tag{24}$$

The homogenized stiffness tensor relates average strain to average stress. It can be obtained with the aid of the strain localization tensor:

$$\begin{aligned} \hat{\underline{\underline{E}}}(p) &= \left\langle \underline{\underline{E}}(\vec{x}, p) : \hat{\underline{\underline{A}}}(\vec{x}, p) \right\rangle \\ &= \left\langle \underline{\underline{E}}(\vec{x}, p) : \hat{\underline{\underline{\varepsilon}}}'(\vec{x}, p) \right\rangle : \left(\hat{\underline{\underline{\varepsilon}}}^{ve}\right)^{-1} = \left\langle \hat{\underline{\sigma}}'(\vec{x}, p) \right\rangle : \left(\hat{\underline{\underline{\varepsilon}}}^{ve}\right)^{-1} = \hat{\underline{\sigma}} : \left(\hat{\underline{\underline{\varepsilon}}}^{ve}\right)^{-1} \end{aligned} \tag{25}$$

where $\underline{\underline{E}}(\vec{x}, p)$ is the LC-transform of the relaxation tensor of the constituent material at the position $\vec{x}$.

The homogenized CTE can be obtained with the aid of the stress concentration tensor:

$$\begin{aligned} \hat{\underline{\alpha}}^{th}(p, T, c) &= \left\langle \underline{\alpha}^{th}(\vec{x}, p, T, c) : \underline{\underline{B}}(\vec{x}, p) \right\rangle \\ &= \left\langle \underline{\alpha}^{th}(\vec{x}, p, T, c) : \hat{\underline{\sigma}}'(\vec{x}, p) \right\rangle : \left(\hat{\underline{\sigma}}\right)^{-1} = \left\langle \underline{w}^{th}(\vec{x}, p, T, c) \right\rangle : \left(\hat{\underline{\sigma}}\right)^{-1} \end{aligned} \tag{26}$$

In the last step of this equation, we define a local energy density $\hat{w}^{th}(\vec{x}, p)$ that is due to the thermal stresses in the material. $\underline{\hat{w}}^{th}(\vec{x}, p)$ is a line vector, of which the i^{th} component is obtained from the solution of the i^{th} elastic FE problem, calculating at each integration point $\vec{x}$

$$\hat{w}_i(\vec{x}, p, T, c) = \underline{\hat{\alpha}}^{th}(\vec{x}, p, T, c) : \underline{\hat{\sigma}}'_i(\vec{x}, p) \tag{27}$$

where $\underline{\hat{\alpha}}^{th}(\vec{x}, p)$ is the LC-transform of the time-dependent CTE of the material at $\vec{x}$ and $\underline{\hat{\sigma}}'_i(\vec{x}, p)$ the local stress tensor at $\vec{x}$ obtained with the i^{th} FE analysis. These equations can be used equivalently to calculate the homogenized CCS and define local energy densities due to the internal stresses caused by chemical shrinkage.

In a thermo-rheologically simple material, in which the relaxation moduli do not depend on strain, temperature T, or degree of cure c (see section 2), the stress concentration tensor $\underline{\underline{\hat{B}}}(\vec{x}, p)$ is independent of strain, T, and c. Hence, in Eqs. (26) and (27) the same stresses $\underline{\underline{\hat{\sigma}}}$ and $\underline{\hat{\sigma}}'_i(\vec{x}, p)$ are used to obtain the LC-transform of the homogenized CTE for any T or c. The LC-transform of the local CTE $\underline{\hat{\alpha}}^{th}(\vec{x}, p, T, c)$ is obtained from the time-dependent CTE of the constituents by means of Eq. (20). Eqs. (26) and (27) are therefore calculated by post-processing operations only, without the need of solving additional FE problems for the different T and c.

The procedure is repeated for M different values of p as explained in section 3.1 and the coefficients of the thermo-viscoelastic behavior in time space are obtained from the inverse LC-transform. Thus, for the whole homogenization procedure, a total of $6M$ linear elastic FE problems have to be solved on the RVE.

3.3. Positive definiteness of stiffness tensors

A viscoelastic model of the generalized Maxwell type only respects the fundamental laws of thermodynamics if the tensors $\underline{\underline{E}}_\infty$ and $\underline{\underline{E}}_k$ are positive definite. This is not necessarily the case for the homogenized behavior obtained with the method of Hirsekorn et al. [2018], because the LC-transform matrix (Eq. 19) is ill-conditioned. As a consequence, the solution of the equation systems (18) and (20) may lead to oscillations in the solution vectors if

plotted against the relaxation times [Hirsekorn et al., 2018]. If these oscillations become too important, they may lead to alternately positive and non-positive definite tensors $\underline{\underline{E}}_k$.

The problem of non-positive definite relaxation tensors is also encountered in an alternative viscoelastic homogenization method [Courtois et al., 2019] that avoids the LC-transform and its inverse. Courtois et al. [2019] determine the average relaxation behavior of an RVE from FE simulations and fit a 3D generalized Maxwell model to the obtained results to identify the coefficients of the $\underline{\underline{E}}_k$. This is done by minimizing a cost function with the condition that the eigenvalues of the $\underline{\underline{E}}_k$ are positive. The positive definiteness of the tensors is checked at each iteration. However, this procedure requires significant computational resources, as many iteration steps have to be skipped because not all tensors are positive definite [Trofimov et al., 2021].

In Hirsekorn et al. [2018] non-positive definite stiffness tensors were avoided by an appropriate choice of the parameters p_i, at which the LC-transform is carried out. Compared to the intuitive choice of setting the p_i equal to the inverse of the relaxation times τ_k, the condition number could be reduced by a factor of 6. While proper results were obtained for the case treated in [Hirsekorn et al., 2018], it is not guaranteed that this approach is sufficient in all cases.

In fact, in order to improve the precision of the homogenization for long relaxation times (at which the only significant differences between the homogenized behavior and the full-scale FE simulations were observed in [Hirsekorn et al., 2018]), we added an additional longer relaxation time ($\tau_N = 10^3$ min) compared to [Hirsekorn et al., 2018] to the constituent and the homogenized behaviors. This relaxation time was omitted in [Hirsekorn et al., 2018], because the associated relative weight in the viscoelastic spectrum of the matrix was very small ($8.8 \cdot 10^{-4}$). Because of this very small contribution to relaxation, adding this element drastically increases the condition number of the LC-transform matrix, leading to some slightly negative eigenvalues of the tensor $\underline{\underline{E}}_N$ associated to the new longer relaxation time τ_N in the homogenized behavior.

This can be avoided using Tikhonov regularization [Tikhonov and Arsenin, 1977] for the least-squares problem. Putting the mn-components ($m, n \in \{1, \ldots, 6\}$) of the tensors $\underline{\underline{E}}_k$ in

Eq. (18) for all k into an N-component vector $\vec{x}_{mn}$ and the mn-components of $\underline{\underline{\hat{E}}}(p_i) - \underline{\underline{E}}_\infty$ for all i into an M-component vector $\vec{b}_{mn}$, Eq. (18) becomes

$$\mathcal{L} \cdot \vec{x}_{mn} = \vec{b}_{mn} \tag{28}$$

A regularization term is added to the least-squares residual. The solution $\vec{x}_{mn}$ is then obtained from the equation system

$$\left(\mathcal{L}^T \cdot \mathcal{P}^T \cdot \mathcal{P} \cdot \mathcal{L} + h\mathcal{S}^T \cdot \mathcal{S}\right) \cdot \vec{x}_{mn} = \mathcal{L}^T \cdot \mathcal{P}^T \cdot \mathcal{P} \cdot \vec{b}_{mn} \tag{29}$$

where $\mathcal{S}$ is a smoothing matrix and $\mathcal{P}$ a preconditioning matrix. We take for $\mathcal{S}$ the $N \times N$ identity matrix, which implies a penalization of the residual by the norm of the solution vector. This has the effect that oscillations in the solution vector are suppressed. For the preconditioning matrix we choose an $M \times M$ diagonal matrix with a larger element on the line corresponding to $p = \infty$, in order to impose a higher precision on the homogenized instantaneous elastic stiffness tensor.

h is the regularization parameter. For $h = 0$ we recover the solution of the non-regularized least-squares problem. The larger h, the more oscillations in the solution vector are penalized, but the more the regularized solution deviates from the optimum least-squares solution. The best choice is therefore the minimum h for which all tensors $\underline{\underline{E}}_k$ are positive definite. Since the solution of Eq. (29) is very fast compared to the solution of the FE problems required for homogenization in the LC-space (section 3.2), we can apply a simple iterative procedure, without significantly increasing the computational costs of the whole homogenization process (which essentially corresponds to the cost of solving $6M$ linear elastic FE problems on the mesh used to represent the RVE and the cost of the post-processings to calculate the volume average of the stresses, the strains, and the energies $\hat{w}_i$, see Eq. (27)). We start from a very small value of $h = 10^{-10}$. If any of the tensors $\underline{\underline{E}}_k$ is not positive definite, we increase h by 1% and calculate a new solution vector and repeat this step until each $\underline{\underline{E}}_k$ is positive definite. In the case of the 3D woven composite presented in the following, $h = 0.00248$ was required for the warp tows, $h = 0.218$ for the weft tows, and no regularization was required at the mesoscopic scale.

4. Application to a 3D woven composite

The proposed homogeniation method is applied to the composite material with a 3D woven interlock reinforcement treated in Hirsekorn et al. [2018]. Two homogenization steps are required: one at the microscopic scale to obtain the homogenized behavior of the consolidated tows, and one at the mesoscopic scale, from which the homogenized behavior of the composite is obtained.

The microscopic RVE contains one cylindrical fiber surrounded by matrix and has a hexagonal cross-section perpendicular to the fiber as shown in [Hirsekorn et al., 2018]. PBC are applied in fiber direction and on opposite sides of the hexagon. The fiber volume fraction in the weft tows is slightly higher (79.6%) than in the warp tows (74.6%). Therefore, two different microscale RVE were generated respecting these two fiber volume fractions, and the homogenization procedure was applied to both microscale RVE to obtain the behavior of the warp and weft tows.

The mesoscopic RVE is the voxel mesh shown in [Hirsekorn et al., 2018]. It was built from μ-CT images of the composite by grayscale segmentation. The fiber volume fractions in the warp and weft tows are calculated from the volume fractions of the warp and weft tows in the voxel mesh, such that they match with the fiber volume fraction of the composite and the weight ratio between the fibers in the warp and weft tows. For each voxel slice of each tow in the plane perpendicular to the tow direction, the material is oriented along the tangent to the center line of the tow at the respective voxel slice. 3D PBC are applied to opposite sides of the mesoscopic RVE as in [Hirsekorn et al., 2018].

At the microscopic scale, the fibers are modeled by a transverse isotropic elastic behavior with the parameters given in [Hirsekorn et al., 2018]. For the matrix, the viscoelastic behavior proposed by Courtois et al. [2018] was used, with the parameters identified in [Hirsekorn et al., 2018]. The experimentally determined relaxation master curves are well represented by a continuous relaxation spectrum [Courtois et al., 2018], sampled by one relaxation time τ_k per decade of time, ranging from 10^{-22} min to 10^{3} min (one longer relaxation time is added compared to [Hirsekorn et al., 2018]). We therefore expect a continuous spectrum

also for the relaxation of the tows and the composite, which we sample by the same relaxation times. These relaxation times refer to the reduced time of the matrix (Eq. 2). Since the homogenization procedure is formulated in terms of the reduced time, the relaxation times of the composite also refer to the reduced time of the matrix.

As explained in section 2, the evolution equations in time of the internal variables can be obtained from the differential equations in terms of the reduced time (Eqs. 8 and 12) by multiplying the relaxation times τ_k with the shift factors a_T (which, in the model of Courtois et al. [2018], depend on temperature and, through T_g, on the degree of cure). Since the homogenized behaviors refer to the same reduced time, the relaxation times of the matrix, the tows, and the composite are all multiplied by the same shift factors in order to obtain the time evolution of the internal variables. Of course, this works only if the reduced times are the same for all constituents, *i.e.,* if the shift factors are the same for all constituents. However, since the fibers are elastic, we can choose the same relaxation times as for the matrix assuming zero relaxation moduli for the fibers. Then, with the assumptions on the relaxation times of the homogenized behavior specified in section 3.1, the homogenized behaviors of the tows have the same shift factors as the matrix, and thus at the mesoscopic scale as well, all constituents have the same shift factors.

The CTE of the fibers and the matrix are assumed to be time-independent, *i.e.,* the tensors $\underline{\alpha}_k^{th}$ in Eq. (9) are zero. The tensor $\underline{\alpha}_\infty^{th}$ then corresponds to the classical, time-independent differential CTE. For the fibers, the CTE are assumed to be independent of temperature between room and cure temperature. However, the CTE in longitudinal and transverse direction are different (Table 1). The CTE of the fully cured matrix is approximately constant between room temperature and T_g, and then changes to a higher value that is again approximately constant between T_g and the curing temperature. For the uncured resin, an approximately constant CTE was observed, which is close to the CTE in the rubbery state. We assume that for intermediate states of cure, the CTE changes linearly with degree of cure. The CCS of the matrix is approximately constant over the whole range of cure. The CTE and CCS of the constituent materials used in the following are summarized in Table 1.

α_L^{th}	α_T^{th}	$\alpha_{\infty,glassy}^{th}(c=1)$
$-0.1 \cdot 10^{-6}$ °C^{-1}	$5.4 \cdot 10^{-6}$ °C^{-1}	$6.73 \cdot 10^{-5}$ °C^{-1}
$\alpha_{\infty,rubbery}^{th}(c=1)$	$\alpha_{\infty}^{th}(c=0)$	α_{∞}^{ch}
$1.80 \cdot 10^{-4}$ °C^{-1}	$1.83 \cdot 10^{-4}$ °C^{-1}	-0.0133

Table 1: CTE of the fiber in longitudinal (L) and transverse (T) direction, CTE of the matrix in glassy, rubbery, and uncured state, and CCS of the matrix.

The homogenized time-dependent CTE of the tows are thus calculated by post-processing as described in section 3.2 using the three different values for the CTE of the matrix. In this way, three different values of the coefficients of $\underline{\alpha}_k^{th}$ and $\underline{\alpha}_{\infty}^{th}$ are obtained for each tow, corresponding to the homogenized time-dependent CTE for the tows with uncured matrix, with fully cured matrix in the rubbery state, and with fully cured matrix in the glassy state. For the CCS only one post-processing is required, as it is assumed to be independent of temperature and cure. At the mesoscopic scale, the homogenized viscoelastic behaviors and the homogenized time-dependent CTE and CCS obtained with the two different microscale RVEs are used for the warp and the weft tows, respectively. The matrix pockets are modeled with the same viscoelastic behavior and with the same time-independent CTE and CCS as at the microscopic scale. The procedure described in section 3 is then applied again to the mesoscopic RVE to obtain the homogenized behavior of the composite.

5. Results

The homogenized behaviors obtained with the method proposed in section 3 are compared with full-scale FE simulations using Z-set [2021]. In each test case presented in the following, the response of the homogenized behavior is calculated on a single integration point. In the corresponding full-scale FE simulations, the same meshes as in the thermo-elastic homogenization steps in the LC-transformed space are used with the thermo-viscoelastic behaviors of the constituents. The evolution of the average strain or stress of the full-scale simulations is then compared to the strain or stress evolution of the homogenized behavior for the same mechanical loading, temperature, or cure conditions. The temperature and cure

variations are applied homogeneously on the whole RVE without any mechanical loading. The viscoelastic behavior is simulated applying an average strain in one direction (tension or shear) on the RVE and leaving the other average strains free.

The homogenization procedure for the viscoelastic behavior is the same as in [Hirsekorn et al., 2018] with the same material properties and RVEs at the micro- and meso-scale. The only difference with respect to [Hirsekorn et al., 2018] is the additional longer relaxation time and the resulting Tikhonov regularization to ensure positive definite relaxation tensors (section 3.3). The homogenized viscoelastic behavior is thus the same as in [Hirsekorn et al., 2018], except for an even better agreement with the full-scale FE simulations for long relaxation times. The results are provided as supplementary material for comparison with [Hirsekorn et al., 2018].

The time-dependent effects of thermal expansion are first validated without taking into account the shift factors (*i.e.,* in terms of reduced times). In the full-scale FE simulations, the temperature at each integration point is increased by 1°C over a very short reduced time step of 10^{-17}min and then kept constant for 10^{3}min. Of course, such a temperature evolution is not realistic. The purpose is to illustrate the time-dependent thermal expansion over the whole spectrum of reduced times. In reality, only part of these mechanisms will be activated at a time, but every part of the spectrum may potentially become active during a cure cycle, depending current value of the shift factors.

Due to viscoelastic effects in the matrix, the average strain of the RVE evolves in time during the constant temperature phase. The evolution is in excellent agreement with the homogenized behavior obtained with the method described in section 3 if exposed to the same temperature. Fig. 1 summarizes the results for the thermal expansion obtained at 27°C (response to a quick temperature increase from 26°C to 27°C) and at 227°C (after a temperature increase from 226°C to 227°C).

The immediate reaction to the temperature change is an expansion in both in-plane and in the out-of-plane direction. However, this expansion is limited by the longitudinal contraction of the fibers and thus smaller in direction of the warp tows than in direction of the weft tows, because there are more fibers in warp than in weft direction. This leads

to in-plane compressive stresses in the matrix, which gradually relax in time. The more these stresses relax, the more the matrix deforms and follows the thermal strain of the fibers. However, this does not affect the volume of the matrix, and therefore the average out-of-plane strain of the composite increases with time (Fig. 1c). Due to the Poisson effect, this amplifies the in-plane contraction caused by the negative longitudinal CTE of the fibers, leading to a sign inversion of the average thermal strains in both warp and weft direction (Fig. 1a and b). The same effects are observed at both temperatures, but are more important in the rubbery state, because the CTE of the matrix is larger than in the glassy state. The time dependence is similar, because the curves are plotted as a function of the reduced time, *i.e.,* the viscoelastic behavior of the matrix is the same in both cases, due to thermo-rheological simplicity (section 2).

The temperature change also causes small average shear strains, because the RVE (which was generated based on tomography images of the real material) is not perfectly orthotropic. As the homogenization procedure is fully anisotropic, the homogenized behavior also reproduces very well the evolution of the shear strains, including the sign changes of the shear strain rates (Fig. 1d and e). At the resulting strain peaks, the only significant differences between the homogenized behavior and the full-scale FE simulations are observed.

The time-dependent effects of chemical shrinkage are evaluated in a similar way by increasing the degree of cure from 0 to 1 at each integration point of the RVE within a reduced time step of 10^{-17}min and then keeping it constant for 10^{3}min. The evolution in time of the average strain over the RVE during the phase of constant degree of cure (shown in Fig. 2) is qualitatively similar to the thermal expansion strain, but with opposite sign. The reason is that like in the case of a temperature change, viscoelastic stress relaxation takes only place in the matrix, but the CCS of the matrix is negative, while its CTE is positive. The curve shapes differ slightly, because while the CCS of the fiber is zero, the CTE of the fiber is much smaller than the CTE of the matrix but not zero. The volume loss of the matrix leads first to a contraction of the composite in all directions, which is partially compensated by the fibers. The more the deviatoric stresses in the matrix relax, the more the volume loss is concentrated to the out-of-plane direction, leading to a flattening of the

composite and a reduction of the tow waviness. This leads to positive in-plane strains (in particular in the warp direction, which contains a higher amount of fibers) at the end of the relaxation phase, even though none of the CCS of the constituents (fiber and matrix) is positive.

In order to verify that the temperature and cure dependence of the viscoelastic behavior is correctly transferred to the homogenized behavior by means of the shift factors, we simulate the strain evolution of a fully cured warp tow when it is heated from room temperature to 200°C at 3°C per minute. Again, we compare full-scale FE simulations on the microscale RVE presented in [Hirsekorn et al., 2018] with the homogenized behavior obtained with the method described in section 3, but this time, the real time is used instead of the reduced time, *i.e.,* the relaxation times of the constituent and the homogenized behaviors are multiplied with the temperature and cure dependent shift factors given in [Hirsekorn et al., 2018]. Fig. 3 shows an excellent agreement between the homogenized behavior and the full-scale FE simulations.

At the beginning of the heating, the matrix is in the glassy state, which limits its deformability. The thermal expansion of the resin in direction of the fibers overcompensates the longitudinal thermal contraction of the fiber, leading to a positive homogenized CTE (Fig. 3a). Due to the mechanical interaction, the fibers are under longitudinal tension, while the matrix is compressed in fiber direction. With increasing temperature, the matrix softens due to the faster relaxation of the deviatoric part of stress. The thermal strain of the tow in fiber direction is thus more and more dominated by the fiber, tending towards the longitudinal CTE of the fiber at high temperatures, where the matrix is in the rubbery state with an approximately elastic behavior with a very low modulus [Courtois et al., 2018; Hirsekorn et al., 2018]. Since the longitudinal thermal strain of the fiber is negative, the initial expansion of the tow gradually slows down and transforms into contraction from about 104°C upwards. This leads to an important negative homogenized differential CTE of the tow in fiber direction. It is caused by the stress relaxation in the matrix, which lets the initially positive thermal strain gradually tend to the negative thermal strain of the fiber between 104°C and T_g. This stress relaxation is due to the viscoelastic behavior of the

matrix and thus not obtained with a thermo-elastic model.

Due to the high stiffness of the fiber and since its CTE is about an order of magnitude smaller than that of the matrix, the major part of the thermal expansion of the matrix is directed into the transverse plane already at low temperatures, leading to a significantly higher transverse CTE of the tow (Fig. 3b). The negative average CTE in fiber direction between 104°C and T_g thus only redirects a comparatively small amount of matrix volume into the transverse plane and the average transverse CTE only slightly increases. A more significant increase is observed at T_g, because at this temperature the CTE of the matrix increases (Table 1). The results obtained for the weft tows with a slightly higher fiber volume fraction are qualitatively similar and not shown here for brevity.

The same simulation is carried out at the mesoscopic scale using the voxelized RVE presented in [Hirsekorn et al., 2018]. For the warp and weft tows, the respective homogenized behaviors are used with the time-dependent CTE and CCS. The relaxation times of all constituent behaviors in the full-scale FE simulations and of the homogenized behavior of the composite are multiplied with the shift factors given in [Hirsekorn et al., 2018] to take into account the influence of temperature on the viscoelastic behavior. All material components are assumed to be fully cured. In Fig. 4 it can be seen that the homogenized behavior of the composite is in excellent agreement with the mesoscopic FE simulations.

In the reinforcement plane, the thermal expansion is dominated by the tows, and similar trends are observed as in the fiber direction of the tows (Fig. 3a). However, since the tows are oriented along two main directions (warp and weft), the thermal expansion of the matrix is confined in both in-plane directions. This leads to a much higher out-of-plane thermal expansion of the composite compared to the in-plane expansions. Due to the higher multiaxiality of the matrix stresses, the relaxation effect becomes dominant at a higher temperature compared to the tows. Since there are more tows in the warp direction, the thermal expansion is more important in the weft direction. In this direction, the maximum thermal strain is reached at a higher temperature (140°C) than in the warp direction (107°C). Due to the biaxial confinement, the stress relaxation leads to an even steeper increase of the out-of-plane strain close to T_g (Fig. 4c). This large out-of-plane strain of the resin increases

the waviness of the tows, leading to a higher in-plane contraction of the composite.

Since the mesoscale RVE is not perfectly orthotropic with respect to the axes of the coordinate system, small shear strains are also generated by the thermal expansion (Fig. 4d). When stress relaxation becomes important, complex evolutions of the average thermal shear strain are observed with multiple slope and sign changes of the effective CTE. The homogenized behavior accurately captures all these evolutions. The only significant differences occur at the sudden sign change of the homogenized in-plane strain rate slightly above the glass transition temperature. This is in line with the results presented in Fig. 1, where the largest differences are also observed around sudden sign changes of the strain rate.

Note that above 160°C, the model predictions become less reliable, because (i) the behavior of the resin is not well identified above T_g (the tests carried out by Courtois et al. [2018] did not provide very reliable results for a soft and unstable resin), (ii) the strains in the resin can be important if it is very soft and thus the small strain linear viscoelastic approach may not be accurate any more, and (iii) there may be direct interaction (such as contact and friction) between the fibers if the resin becomes very soft, which is not taken into account in the model.

6. Conclusions

The presented FE simulations show that the temperature (and cure) dependent stress relaxation in the polymer matrix leads to complex evolutions of the average thermal strain of polymer composites when they are heated with possible sign changes of the apparent CTE, depending on the architecture of the fiber reinforcement. Another consequence is a delayed evolution of thermal strain at constant temperature caused by a previous temperature change. Similar effects are expected for chemical shrinkage. These effects can be modeled by time-dependent CTE and CCS, based on a formulation inspired by the classical generalized Maxwell model for viscoelastic behaviors. It corresponds to a Prony decomposition of the time-dependent CTE and CCS. Like in the case of viscoelasticity, for each Prony element a strain-like internal variable is added to the model, which respectively accounts for the history of temperature or degree of cure the material has experienced.

The homogenization procedure for viscoelastic behaviors proposed in [Hirsekorn et al., 2018] was extended to thermal expansion and chemical shrinkage. The method is compatible with the proposed formulation of time-dependent expansion coefficients. It was shown that for constituent materials with time-independent CTE and CCS, the viscoelastic behavior of at least one of the constituents leads to time-dependent homogenized CTE and CCS.

The resulting homogenized viscoelastic behavior is thermodynamically consistent if the stiffness tensors associated to the Maxwell elements are all positive definite. In addition to the choice of the LC-parameters, at which the thermo-elastic homogenization in the LC-space is carried out [Hirsekorn et al., 2018], Tikhonov regularization can be applied to the inverse LC-transform, in order to suppress oscillations in the homogenized viscoelastic spectrum, which may cause non-positive definite stiffness tensors. The homogenized behavior is in excellent agreement with the average stress and strain evolutions obtained with full-scale FE simulations covering the whole relaxation time spectrum and the temperature range of typical cure cycles. This shows that through the internal variables, the homogenized behavior takes into account all the viscoelastic, thermal expansion, and chemical shrinkage effects of the whole RVE.

The simulation of the evolution of thermal strain while heating a composite from room temperature to well above the glass transition temperature of the polymer matrix shows some interesting effects caused by the stress relaxation in the polymer matrix. These time-dependent effects can have a significant impact on the residual stress formation in composites and are neglected if time-independent homogenized CTE and CCS are used. In particular, the sign change of the average differential CTE of the composite caused by the stress relaxation close to the glass transition temperature of the resin would not be obtained by purely thermo-elastic homogenization with temperature-independent CTEs of the constituents without taking into account the viscoelastic behavior of the matrix.

Future work will consist of comparing the predicted effects with experimental observations of the average thermal expansion and chemical shrinkage of textile composites with complex reinforcement architectures. Particular attention will be given to the time-dependent effects that cause an evolution of the shape of composites even at constant tem-

perature or after the polymerization has been stopped. It is also planned to use the proposed methodology in multi-scale simulations of the formation of residual stresses in textile composites during the curing process and to predict the final shape of composite parts. This procedure can also give indications on whether the part shape will evolve in time after the end of the curing process. It may thus help to tackle these important questions of the design process of composite structures.

Appendix A. Incremental procedure of the thermo-viscoelastic behavior

To calculate the evolution of the internal variables of the thermo-viscoelastic behavior presented in section 2 over a time step in a FE simulation, first the increment of the thermal strain is calculated (Appendix A.1). The increment of the chemical strain is obtained using the same procedure. These strains are subtracted from the increment of the total strain, yielding the increment of the viscoelastic strain. The viscoelastic strain is then used to calculate the increments of the internal variables of the viscoelastic behavior and the stress at the end of the time step (Appendix A.2).

Appendix A.1. Thermal strain

The evolution of the internal variables of thermal strain in time is obtained from Eq. (12) using the definition of the reduced time given in Eq. (2)

$$\dot{\underline{\varepsilon}}_k^{th}(t) = \underline{\alpha}_k^{th}(T(t), c(t))\dot{T}(t) - \frac{1}{a_T(t)\tau_k}\underline{\varepsilon}_k^{th}(t) \tag{A.1}$$

We integrate this equation over a time step from $t = t_{n-1}$ to $t = t_n$, approximating the shift factor by its value at $\frac{1}{2}\left(a_T\left(t_{n-1}\right) + a_T\left(t_n\right)\right)$, *i.e.,* by the shift factor corresponding to the average temperature and degree of cure over the time step (simply noted a_T in the following). The evolution of the coefficients $\underline{\alpha}_k^{th}$ is approximated by a linear function with time over the time step, *i.e.,*

$$\underline{\alpha}_k^{th}(t) = \frac{t_n - t}{\Delta t_n}\underline{\alpha}_k^{th}(t_{n-1}) + \frac{t - t_{n-1}}{\Delta t_n}\underline{\alpha}_k^{th}(t_n) \tag{A.2}$$

with $\Delta t_n = t_n - t_{n-1}$.

The temperature is given as an external parameter an is known at the different time steps. Over each time step, we interpolate it linearly, such that

$$\dot{T} = \frac{\Delta T_n}{\Delta t_n} \tag{A.3}$$

between $t = t_{n-1}$ and $t = t_n$ with $\Delta T = T(t_n) - T(t_{n-1})$.

If the value of the internal variable at the beginning of the time step is known (from the last time increment), we then obtain the following expression for the internal variable at the end of the time step

$$\underline{\varepsilon}_k^{th}(t_n) = \mathrm{e}^{-\frac{\Delta t_n}{a_T \tau_k}} \underline{\varepsilon}_k^{th}(t_{n-1}) + \mathrm{e}^{-\frac{t_n}{a_T \tau_k}} \int_{t_{n-1}}^{t_n} \underline{\alpha}_k^{th}(t) \mathrm{e}^{\frac{t}{a_T \tau_k}} \frac{\Delta T_n}{\Delta t_n} dt \tag{A.4}$$

The remaining integral can be solved analytically if we use the approximation of Eq. (A.2) for $\underline{\alpha}_k^{th}(t)$. It is then

$$\begin{aligned} \underline{\varepsilon}_k^{th}(t_n) - \underline{\varepsilon}_k^{th}(t_{n-1}) = {} & \frac{a_T \tau_k}{\Delta t_n} \left(1 - \mathrm{e}^{-\frac{\Delta t_n}{a_T \tau_k}}\right) \left(\underline{\alpha}_k^{th}(t_{n-1}) \Delta T_n - \frac{\Delta t_n}{a_T \tau_k} \underline{\varepsilon}_k^{th}(t_{n-1})\right) \\ & + \frac{a_T \tau_k}{\Delta t_n} \left(1 - \frac{a_T \tau_k}{\Delta t_n} \left(1 - \mathrm{e}^{-\frac{\Delta t_n}{a_T \tau_k}}\right)\right) \left(\underline{\alpha}_k^{th}(t_n) - \underline{\alpha}_k^{th}(t_{n-1})\right) \Delta T_n \end{aligned} \tag{A.5}$$

The terms in $\frac{a_T \tau_k}{\Delta t_n}$ are calculated using the power series expansion of the exponential function. In the first factor in Eq. (A.5), the first term of the power series vanishes, *i.e.,*

$$\frac{a_T \tau_k}{\Delta t_n} \left(1 - \mathrm{e}^{-\frac{\Delta t_n}{a_T \tau_k}}\right) = \sum_{i=0}^{\infty} \frac{\left(-\frac{\Delta t_n}{a_T \tau_k}\right)^i}{(i+1)!} \tag{A.6}$$

and in the second factor, the first to terms of the power series vanish, *i.e.,*

$$\frac{a_T \tau_k}{\Delta t_n} \left(1 - \frac{a_T \tau_k}{\Delta t_n} \left(1 - \mathrm{e}^{-\frac{\Delta t_n}{a_T \tau_k}}\right)\right) = \sum_{i=0}^{\infty} \frac{\left(-\frac{\Delta t_n}{a_T \tau_k}\right)^i}{(i+2)!} \tag{A.7}$$

Using these series, the factors in Eq. (A.5) can be accurately calculated even for $\frac{a_T \tau_k}{\Delta t_n}$ close to zero, which otherwise would lead to significant numerical errors due to subtraction of almost equal numbers.

We see from Eq. (13) after replacing the deriative in reduced time by the time derivative that

$$\dot{\underline{\varepsilon}}^{th}(t) = \underline{\alpha}_{\infty}^{th}(T(t), c(t)) \dot{T}(t) - \dot{\underline{\varepsilon}}_k^{th}(t) \tag{A.8}$$

Supposing for $\underline{\alpha}_{\infty}^{th}$ a linear evolution in time over the time step as in Eq. (A.2) for the $\underline{\alpha}_{k}^{th}$, we integrate the thermals train over the time step, which yields

$$\underline{\varepsilon}^{th}(t_n) - \underline{\varepsilon}^{th}(t_{n-1}) = \frac{1}{2}\left(\underline{\alpha}_{\infty}^{th}(t_n) - \underline{\alpha}_{\infty}^{th}(t_{n-1})\right)\Delta T_n - \sum_{k=1}^{N}\left(\underline{\varepsilon}_{k}^{th}(t_n) - \underline{\varepsilon}_{k}^{th}(t_{n-1})\right) \tag{A.9}$$

From this increment of the thermal strain over the time step, the thermal strain at the end of the time step can be calculated. The same procedure is applied to obtain the chemical strain at the end of the time step. Subtracting both from the total strain, the viscoelastic strain at the end of the time step $\underline{\varepsilon}^{ve}(t_n)$ is obtained.

Appendix A.2. Viscoelastic behavior

The integration of the internal variables of the viscoelastic behavior over the time step follows the same principle as for the internal variables of the thermal and the chemical strain. Setting the shift factor a_T equal to its value at the middle of the time step, and assuming a linear evolution of the viscoelastic strain over the time step, the increment of the viscoelastic internal variables is obtained by integration of Eq. (8) over the time step

$$\begin{aligned}\underline{\varepsilon}_{k}^{ve}(t_n) - \underline{\varepsilon}_{k}^{ve}(t_{n-1}) = &\left(1 - \mathrm{e}^{-\frac{\Delta t_n}{a_T \tau_k}}\right)\left(\underline{\varepsilon}^{ve}(t_{n-1}) - \underline{\varepsilon}_{k}^{ve}(t_{n-1})\right) \\ &+ \left(1 - \frac{a_T \tau_k}{\Delta t_n}\left(1 - \mathrm{e}^{-\frac{\Delta t_n}{a_T \tau_k}}\right)\right)\frac{\underline{\varepsilon}^{ve}(t_n) - \underline{\varepsilon}^{ve}(t_{n-1})}{\Delta t_n}\end{aligned} \tag{A.10}$$

Here again, we calculate the terms in $\frac{a_T \tau_k}{\Delta t_n}$ using Eqs. (A.6) and (A.7). From these increments, we can calculate the values of the internal variables $\underline{\varepsilon}_{k}^{ve}$ at the end of the time step. Eq. (7) with the viscoelastic strain at the end of the time step obtained in Appendix A.1 gives then the stress at the end of the time step.

This incremental procedure only gives accurate results if the shift factor and the coefficients $\underline{\alpha}_{\infty}^{th}$ and $\underline{\alpha}_{k}^{th}$ and their chemical counterparts do not vary much over the time step. Since all these coefficients depend on temperature and degree of cure, the time steps in the FE simulations have to be adjusted such that these parameters do not change much over a time step.

Acknowledgements

The research presented in this article was funded by the Safran Group, France.

References

S. R. White, Y. K. Kim, Process-induced residual stress analysis of AS4/3501-6 composite material, Mechanics of Composite Materials and Structures 5 (1998) 153–186.

M. Wisnom, M. Gigliotti, N. Ersoy, M. Campbell, K. Potter, Mechanisms generating residual stresses and distortion during manufacture of polymer-matrix composite structures, Composites Part A-Applied Science and Manufacturing 37 (2006) 522–529.

N. Zobeiry, A. Forghani, C. Li, K. Gordnian, R. Thorpe, R. Vaziri, G. Fernlund, A. Poursartip, Multiscale characterization and representation of composite materials during processing, Philosophical Transactions of the Royal Society A: Mathematical, Physical and Engineering Sciences 374 (2016) 20150278.

J. Russell, M. Madhukar, M. Genidy, A. Lee, New method to reduce cure-induced stresses in thermoset polymer composites, Part III: Correlating stress history to viscosity, degree of cure, and cure shrinkage, Journal of Composite Materials 34 (2000) 1926–1947.

C. Billotte, F. Bernard, E. Ruiz, Chemical shrinkage and thermomechanical characterization of an epoxy resin during cure by a novel in situ measurement method, European Polymer Journal 49 (2013) 3548–3560.

D. O'Brien, P. Mather, S. White, Viscoelastic properties of an epoxy resin during cure, Journal of Composite Materials 35 (2001) 883–904.

M. Zarrelli, A. Skordos, I. Partridge, Toward a constitutive model for cure-dependent modulus of a high temperature epoxy during the cure, European Polymer Journal 46 (2010) 1705–1712.

A. Courtois, M. Hirsekorn, M. Benavente, A. Jaillon, L. Marcin, E. Ruiz, M. Lévesque, Viscoelastic behavior of an epoxy resin during cure below the glass transition temperature: Characterization and modeling, Journal of Composite Materials 53 (2018) 155–171.

Y. K. Kim, S. R. White, Stress relaxation behavior of 3501-6 epoxy resin during cure, Polymer Engineering & Science 36 (1996) 2852–2862.

A. Johnston, R. Vaziri, A. Poursartip, A Plane Strain Model for Process-Induced Deformation of Laminated Composite Structures, Journal of Composite Materials 35 (2001) 1435–1469.

J. Svanberg, J. Holmberg, Prediction of shape distortions Part I. FE-implementation of a path dependent constitutive model, Composites Part A-Applied Science and Manufacturing 35 (2004) 711–721.

N. Zobeiry, R. Vaziri, A. Poursartip, Computationally efficient pseudo-viscoelastic models for evaluation of residual stresses in thermoset polymer composites during cure, Composites Part A-Applied Science and Manufacturing 41 (2010) 247–256.

M. Benavente, L. Marcin, A. Courtois, M. Lévesque, E. Ruiz, Viscoelastic distortion in asymmetric plates during post curing, Composites Part A: Applied Science and Manufacturing 103 (2017) 122–130.

J. Zhang, M. Zhang, S. Li, M. Pavier, D. Smith, Residual stresses created during curing of a polymer matrix composite using a viscoelastic model, Composites Science and Technology 130 (2016) 20–27.

A. Ding, S. Li, J. Sun, J. Wang, L. Zu, A thermo-viscoelastic model of process-induced residual stresses in composite structures with considering thermal dependence, Composite Structures 136 (2016) 34–43.

M. Benavente, L. Marcin, A. Courtois, M. Lévesque, E. Ruiz, Numerical analysis of viscoelastic process-induced residual distortions during manufacturing and post-curing, Composites Part A: Applied Science and Manufacturing 107 (2018) 205–216.

M. Hirsekorn, L. Marcin, T. Godon, Multi-scale modeling of the viscoelastic behavior of 3D woven composites, Composites Part A: Applied Science and Manufacturing 112 (2018) 539–548.

A. Courtois, L. Marcin, M. Benavente, E. Ruiz, M. Lévesque, Numerical multiscale homogenization approach for linearly viscoelastic 3D interlock woven composites, International Journal of Solids and Structures 163 (2019) 61–74.

A. Trofimov, J. Le-Pavic, C. Ravey, W. Albouy, D. Therriault, M. Lévesque, Multi-scale modeling of distortion in the non-flat 3D woven composite part manufactured using resin transfer molding, Composites Part A: Applied Science and Manufacturing 140 (2021) 106145.

M. A. Zocher, S. E. Groves, D. H. Allen, A three-dimensional finite element formulation for thermoviscoelastic orthotropic media, International Journal for Numerical Methods in Engineering 40 (1997) 2267–2288.

S. Sawant, A. Muliana, A thermo-mechanical viscoelastic analysis of orthotropic materials, Composite Structures 83 (2008) 61–72.

H. Pettermann, A. DeSimone, An anisotropic linear thermo-viscoelastic constitutive law: Elastic relaxation and thermal expansion creep in the time domain, Mechanics of Time-Dependent Materials 22 (2018) 421–433.

Z. BaÅ$\frac{3}{4}$ant, Delayed thermal dilatations of cement paste and concrete due to mass transport, Nuclear Engineering and Design 14 (1970) 308–318.

S. Park, R. Schapery, Methods of interconversion between linear viscoelastic material functions. Part I - A numerical method based on Prony series, International Journal of Solids and Structures 36 (1999) 1653–1675.

R. Schapery, S. Park, Methods of interconversion between linear viscoelastic material functions. Part II - An approximate analytical method, International Journal of Solids and Structures 36 (1999) 1677–1699.

M. Hirsekorn, F. Petitjean, A. Deramecourt, A continuous threshold model for the visco-elasto-plastic behavior of PET based multi-layer polymeric films, Mechanics of Time-Dependent Materials 14 (2010) 25–45.

M. Hirsekorn, F. Petitjean, A. Deramecourt, A semi-analytical integration method for the numerical simulation of nonlinear visco-elasto-plastic materials, Mechanics of Time-Dependent Materials 15 (2011) 139–167.

S. Beurthey, A. Zaoui, Structural morphology and relaxation spectra of viscoelastic heterogeneous materials, European Journal of Mechanics - A/Solids 19 (2000) 1–16.

M. Lévesque, M. D. Gilchrist, N. Bouleau, K. Derrien, D. Baptiste, Numerical inversion of the Laplace-Carson transform applied to homogenization of randomly reinforced linear viscoelastic media, Computational Mechanics 40 (2007) 771–789.

A. N. Tikhonov, V. I. Arsenin, Solutions of ill-posed problems, volume 14, Winston, Washington, DC, 1977.

Z-set, Non-linear material & structure analysis suite, 2021. URL: `http://www.zset-software.com/`.

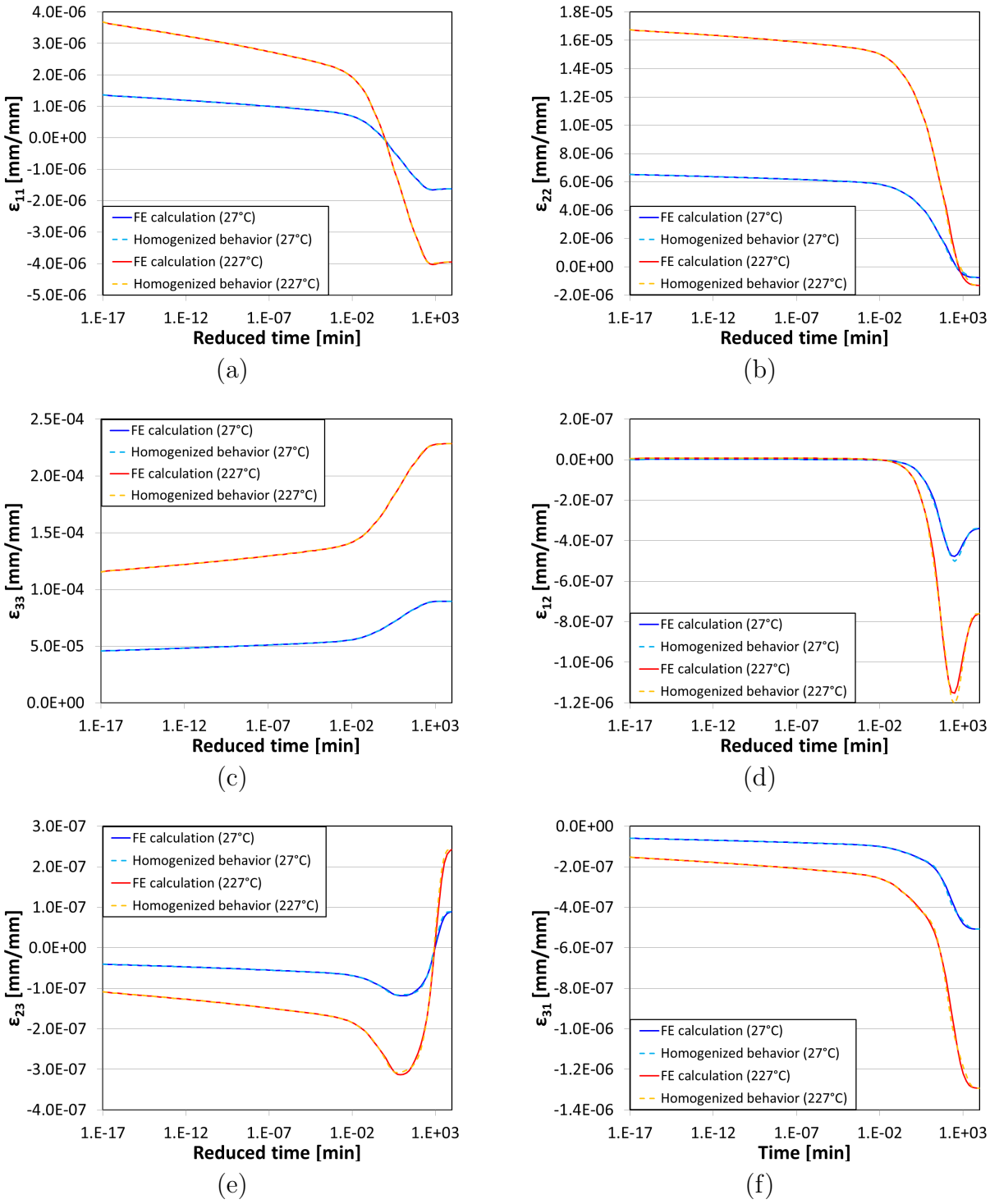

Figure 1: Comparison between the strain evolution of the homogenized time-dependent CTE and the full-scale FE simulation after rapid temperature increases by 1°C around 27°C and 227°C. Index 1 refers to the warp, index 2 to the weft, and index 3 to the out-of-plane direction.

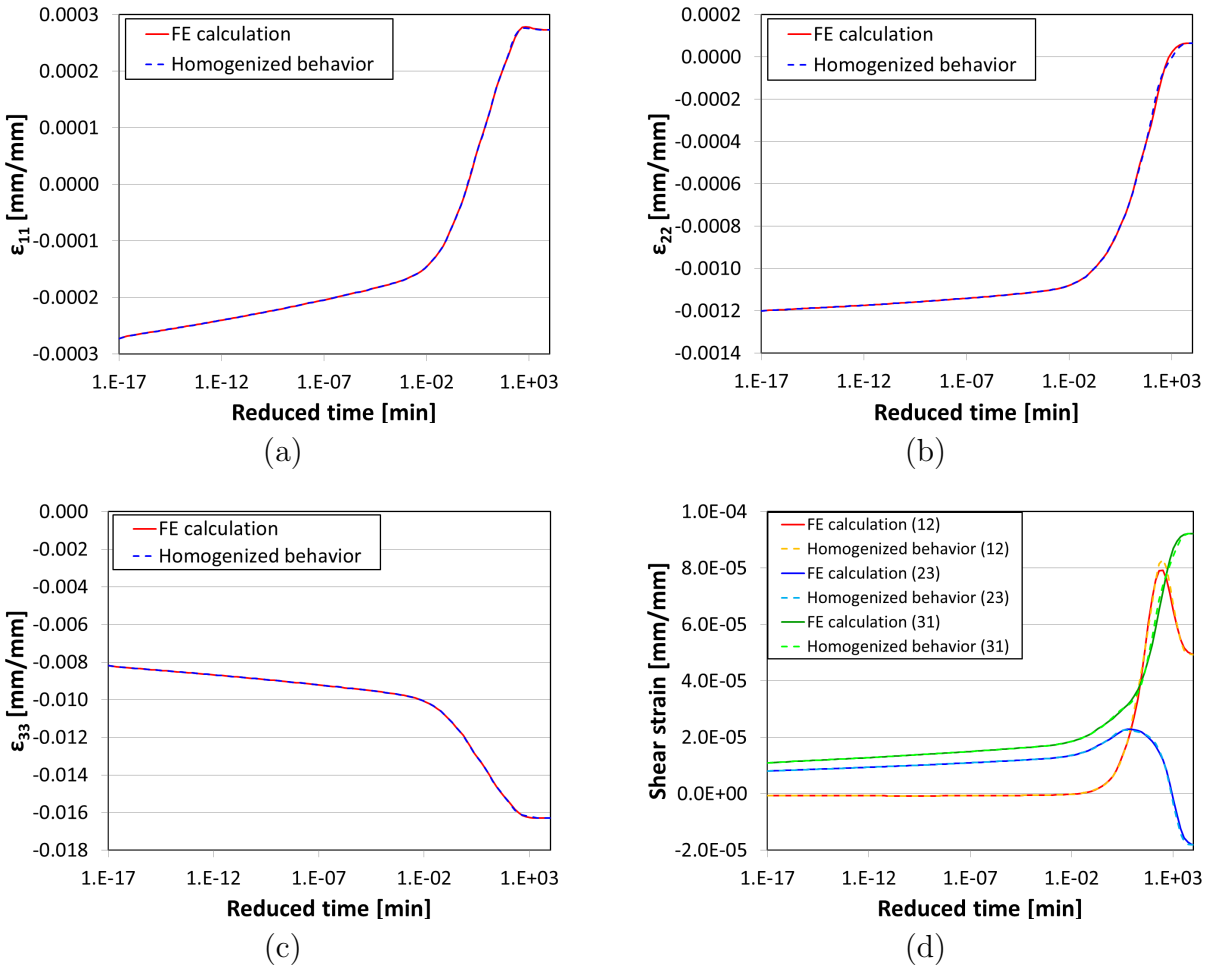

Figure 2: Comparison between the strain evolution of the homogenized time-dependent CCS and the full-scale FE simulation after a rapid change of cure from 0 to 1: strain in (a) warp (1), (b) weft (2), and (c) out-of-plane (3) direction, (d) shear strains.

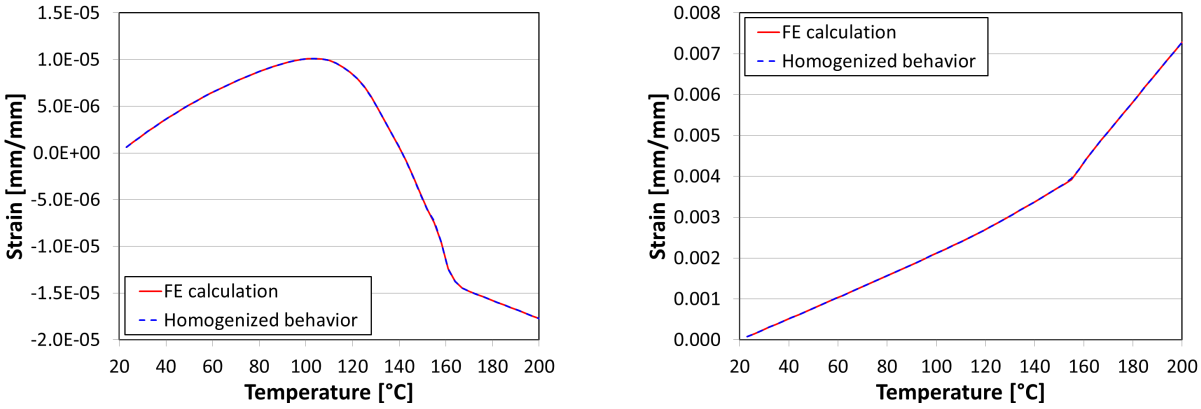

Figure 3: Comparison between the strain evolution of a fully cured warp tow during a temperature increase of 3°C per minute obtained with full-scale FE simulations and with the homogenized thermo-viscoelastic behavior: (a) strain in direction of the fiber, (b) strain transverse to the fibers.

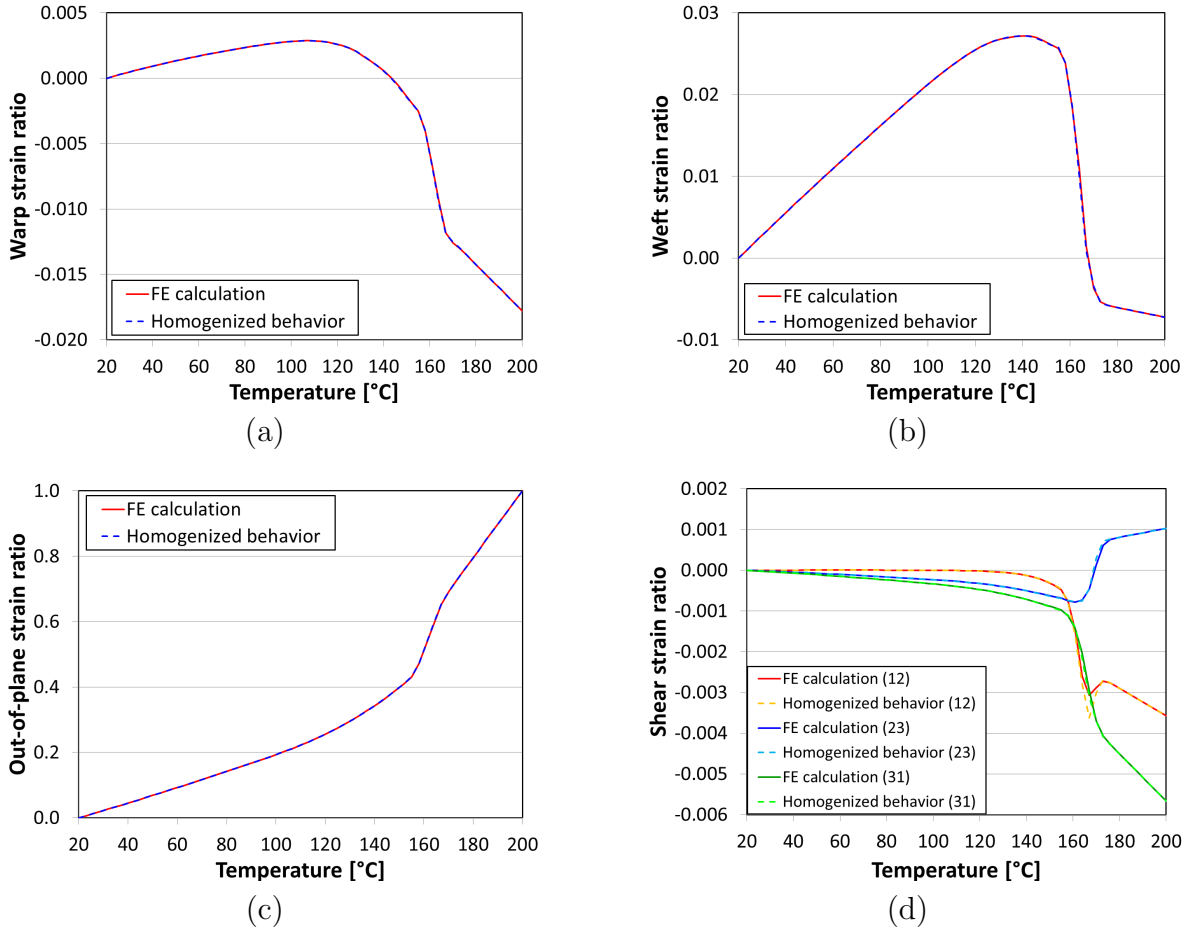

Figure 4: Comparison between ratio of the average strain components of the fully cured composite and the final out-of-plane strain at 200°C during a temperature increase of 3°C per minute obtained with full-scale FE simulations and with the homogenized thermo-viscoelastic behavior: (a) warp, (b) weft, (c) out-of-plane and, (d) shear components (warp=1, weft=2, out-of-plane=3).

CRediT authorship contribution statement

Martin Hirsekorn: Conceptualization, Methodology, Software, Formal analysis, Writing - Original Draft, Visualization.

Lionel Marcin: Resources, Writing - Review & Editing.

Thierry Godon: Resources, Writing - Review & Editing.

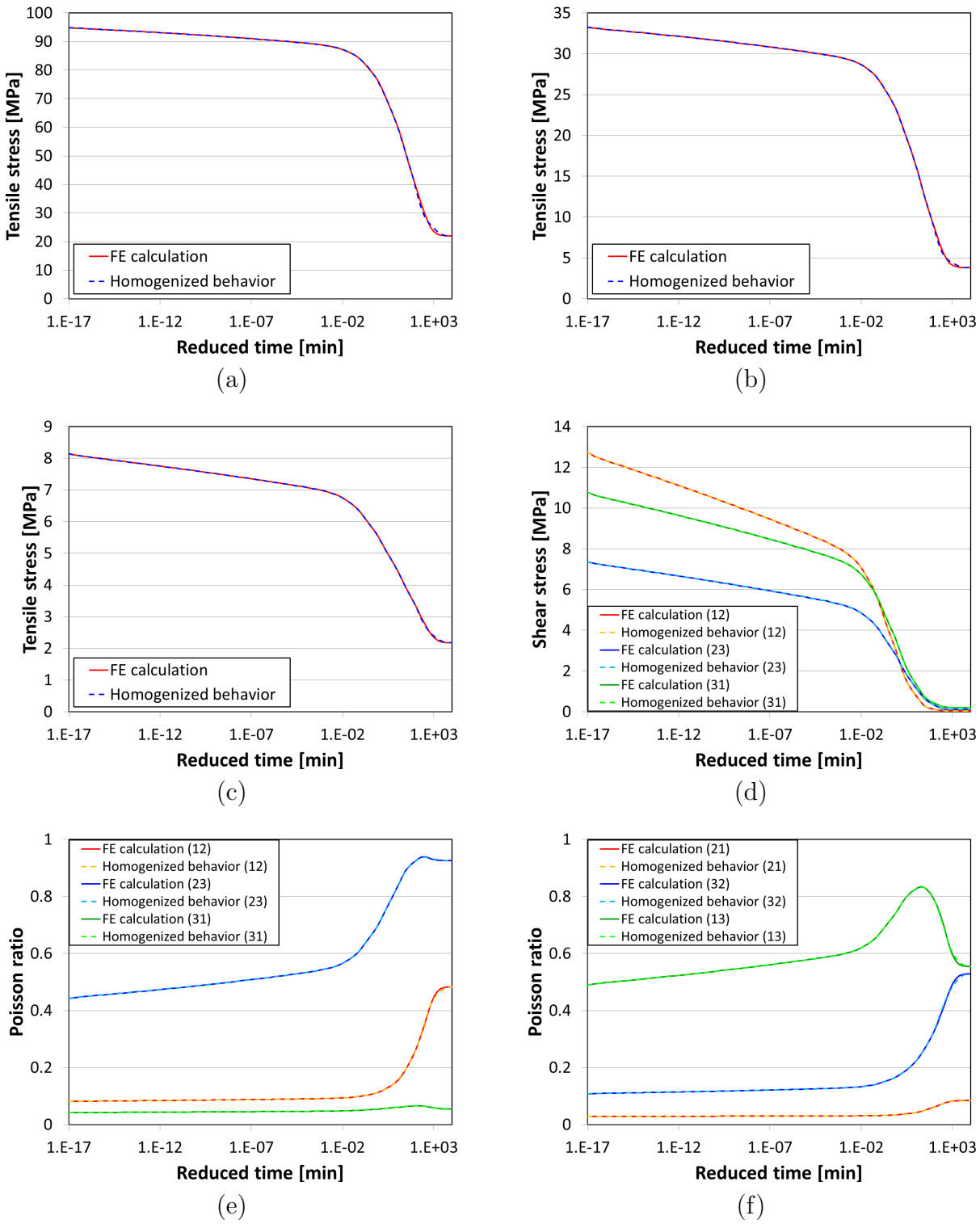

Figure S1: Comparison between the stress response of the homogenized viscoelastic model of the composite and the full-scale FE simulation: stress in loading direction under constant tensile strain in (a) warp, (b) weft, and (c) out-of-plane direction, (d) shear stress evolution under constant shear strain, and (e) and (f) evolution of the Poisson ratios under constant tensile strain.